Supplementary Information for ALD-Engineered Amorphous NiO/Crystalline CoFe-PBA Heterointerface for High-Performance Seawater Oxygen Evolution

*Jie Tan [a], Mingliang Guo [b, *], Hai Li [a], Yongcheng Qi [a], Mingyu Wang [a], Xiaohong Wang [a], Hualan Li [c, *], Lei Ding [a, *]*

[a] State Key Laboratory of Tropic Ocean Engineering Materials and Materials Evaluation, School of Materials Science and Engineering, Hainan University, Haikou 570228, China. E-mail: lding@hainanu.edu.cn

[b] School of Automotive Materials, Hubei University of Automotive Technology, Shiyan 442002, China. E-mail: guomingliang02@163.com

[c] School of Chemistry and Materials Engineering, Mianyang Teachers' College, Mianyang 621000, China. E-mail: scmyli789@aliyun.com

Experimental Section

Materials: Trisodium citrate dihydrate ($C_6H_5Na_3O_7·2H_2O$, AR) was purchased from Xilong Scientific Co., Ltd. Potassium ferricyanide ($K_3Fe(CN)_6$, ≥ 99.5%), Iron(III) nitrate nonahydrate ($Fe(NO_3)_3·9H_2O$, 98.5%), Cobalt nitrate hexahydrate ($Co(NO_3)_2·6H_2O$, 99%) and Bis(cyclopentadienyl)nickel(II) ($Ni(C_5H_5)_2$, 98%) were purchased from Macklin. The nickel foam (NF) used as a substrate was obtained from Suzhou Sinero Technology Co., Ltd.

Preparation of CoFe-PBA/NF: Firstly, $Na_3C_6H_5O_7·2H_2O$ (1.125 mmol), $K_3Fe(CN)_6$ (1 mmol), $Fe(NO_3)_3·9H_2O$ (0.5 mmol) and $Co(NO_3)_2·6H_2O$ (0.5 mmol) were dissolved in deionized water (50 mL) and stirred continuously for 5 h. Then, the product was collected by centrifugation, washed repeatedly with ethanol and dried. Finally, 5 mg of CoFe-PBA was dispersed in ethanol (1 mL), sonicated for 1 h, and then 500 uL of the slurry was dropped on both sides of the nickel foam (1 cm × 1.5 cm).

Preparation of NiO/CoFe-PBA/NF and NiO/NF: $Ni(C_5H_5)_2$ and H_2O as precursors. NiO was deposited on the surface of CoFe-PBA/NF by ALD system (**Fig. S1**) to form NiO/CoFe-PBA/NF catalyst. The ALD process was conducted at a deposition temperature of 200 °C for 50 cycles. The parameters for the ALD system are as follows: Valve A: 10000 ms, Valve B: 10000 ms, Valve C: 10000 ms, Valve D: 2000 ms. The related reaction of the ALD process is as follows: $C_5H_5\text{-}Ni\text{-}C_5H_5 + H_2O \rightarrow NiO + C_5H_6 + C_5H_6$. The precursor was purged into the deposition chamber with inert gases (argon and nitrogen), and $Ni(C_5H_5)_2$ reacted with water to form an atomic film. The preparation process of NiO/NF is similar, except that CoFe-PBA/NF is replaced with NF.

Characterization: The XRD results were achieved using a LabX XRD-6100 X-ray diffractometer with Cu Kα radiation (40 kV, 30 mA). The Raman spectra were collected on Horiba Labram HR800 Evolution spectrometer with a 532 nm excitation laser. X-ray photoelectron spectroscopy (XPS) was performed on a Kratos Amicus X-ray photoelectron spectrometer. The scanning electron microscopy (SEM) results were collected by an SU8010 at an accelerating voltage of 5.0 kV. Transmission electron microscopy (TEM) images were collected using JEM2100F installation. The elemental mapping of the samples was performed using an energy-dispersive X-ray spectroscopy accessory attached to the TEM.

Electrochemical measurements: Electrochemical analysis was performed using a Bio-Logical VMP-300 electrochemical workstation with a standard three-electrode configuration. The NiO/NF, CoFe-PBA/NF, and NiO/CoFe-PBA/NF catalysts were used as the working electrodes, with a graphite rod counter electrode and a reference electrode (Hg/HgO). The electrolyte was a 1.0 M KOH solution and 1.0 M KOH with seawater. The seawater was sourced from the Baishamen sea area, Hainan Province, China. The linear sweep voltammetry (LSV) for OER was measured at the scan rate of 5 mV s^{-1} with the iR compensation (85%). The measured potential was normalized by the reversible hydrogen electrode (RHE) according to the equation: $E_{RHE}=E_{Hg/HgO}$ + 0.098 V + 0.059 pH. The electrochemical impedance spectra (EIS) were measured from 0.01 Hz to 100 kHz at 1.524 V vs. RHE for OER. The electrochemical active surface area (ECSA) was tested in the non-Faraday region. Chronopotentiometry was used to measure the long-term stability of OER.

Computational details: All the calculations are performed in the framework of the density functional theory with the projector augmented plane-wave method, as implemented in the Vienna ab initio simulation package.[1] We used the generalized gradient approximation (GGA) with the Pedrew-Burke-Ernzerhof (PBE) function and Hubbard U corrections (4.30, 3.52, 3.80 eV for treating Fe, Co and Ni 3d orbitals) were introduced to consider the self-interaction error of transition metals.[2,3] The cut-off energy for plane wave is set to 500 eV. The energy criterion is set to 10^{-5} eV in iterative solution of the Kohn-Sham equation. The vacuum layer of 15 Å is added perpendicular to the sheet to avoid artificial interaction between periodic images. The Brillouin zone integration is performed using a 2x2x1 k-mesh. All the structures are relaxed until the residual forces on the atoms have declined to less than 0.01 eV/Å.

Fig. S1. Digital photograph of ALD-GSL-4.

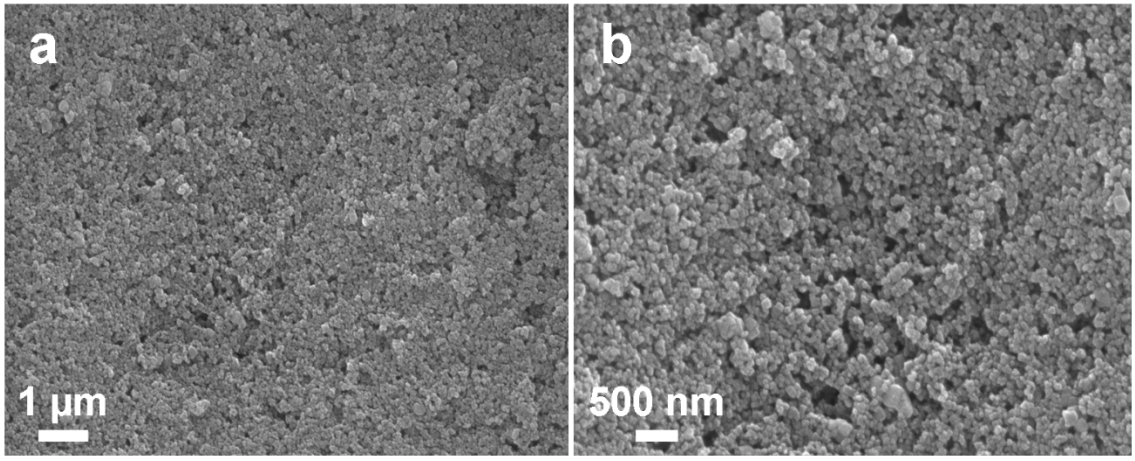

Fig. S2. SEM images of CoFe-PBA/NF.

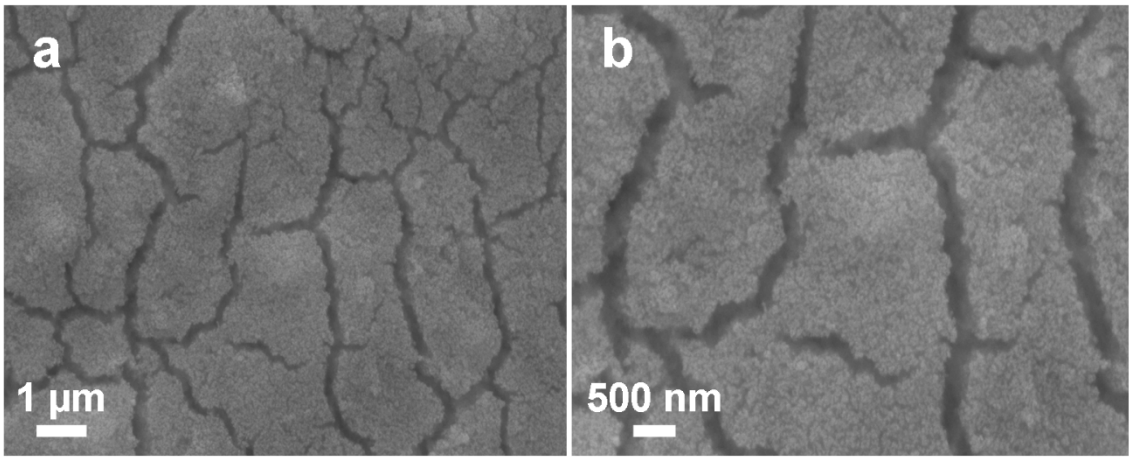

Fig. S3. SEM images of NiO/CoFe-PBA/NF.

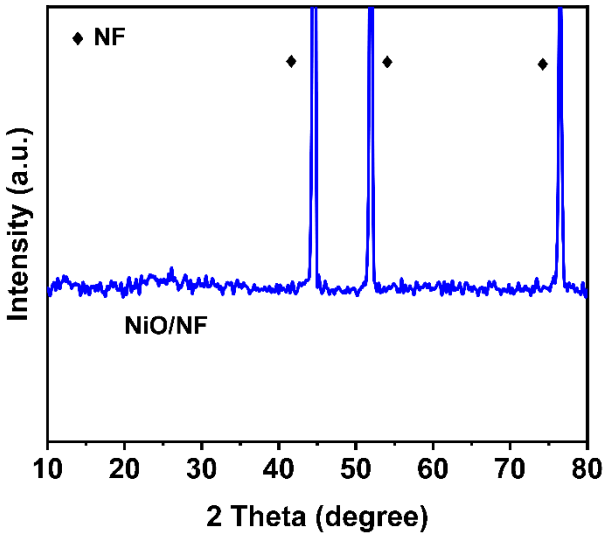

Fig. S4. XRD pattern of NiO/NF.

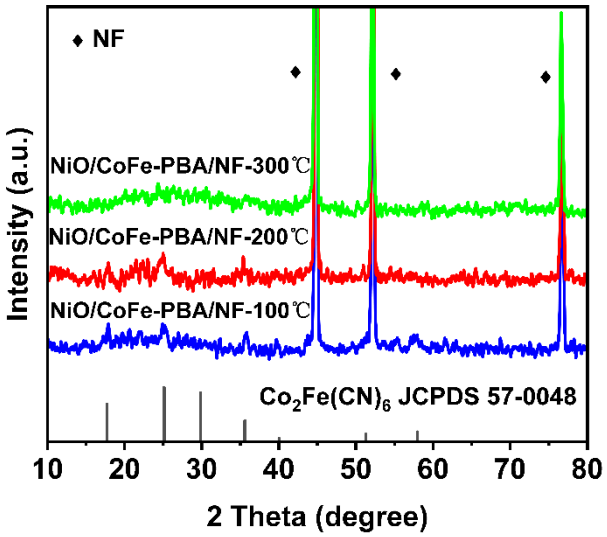

Fig. S5. XRD patterns of NiO/CoFe-PBA/NF at various temperatures.

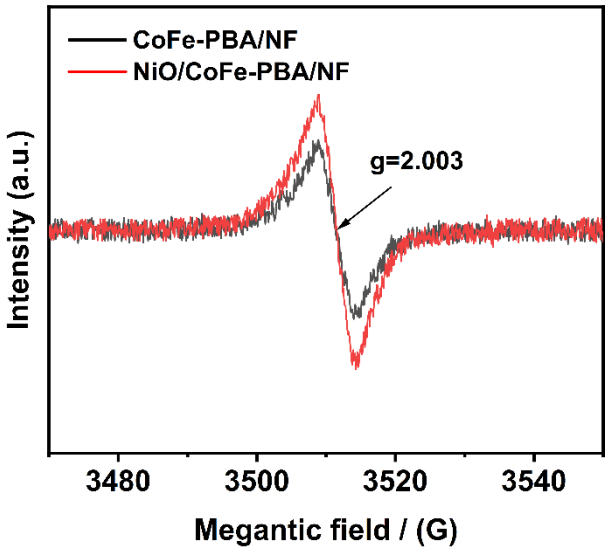

Fig. S6. EPR spectra of CoFe-PBA/NF and NiO/CoFe-PBA/NF.

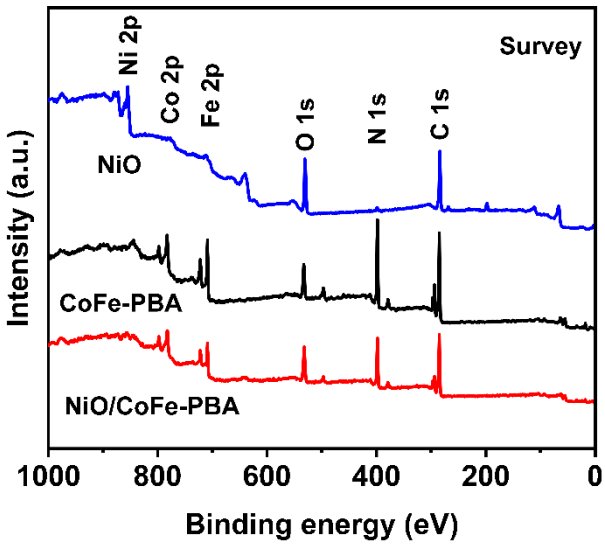

Fig. S7. XPS survey spectra of NiO/NF, CoFe-PBA/NF, and NiO/CoFe-PBA/NF.

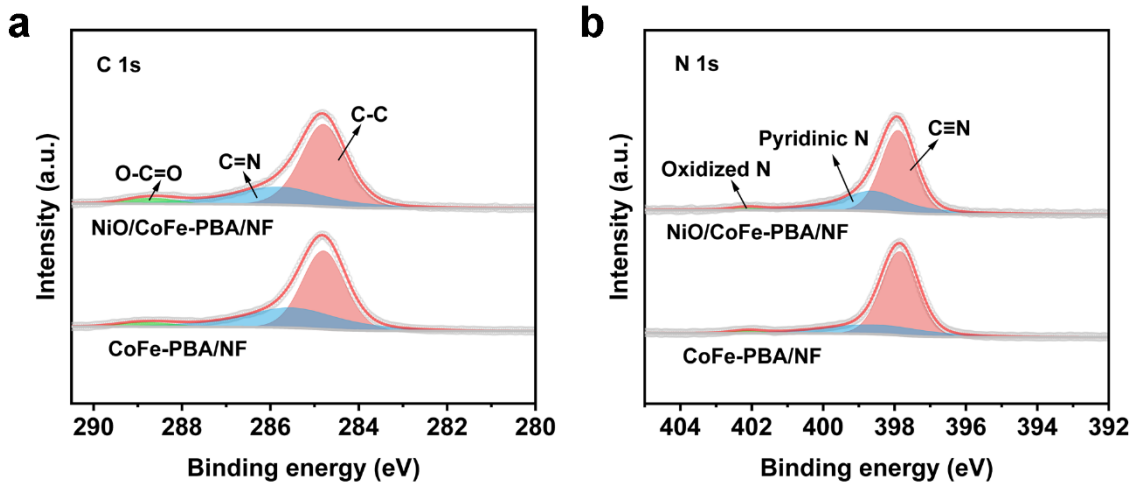

Fig. S8. High-resolution XPS spectra of NiO/NF, CoFe-PBA/NF, and NiO/CoFe-PBA/NF. a) C 1s, and b) N 1s.

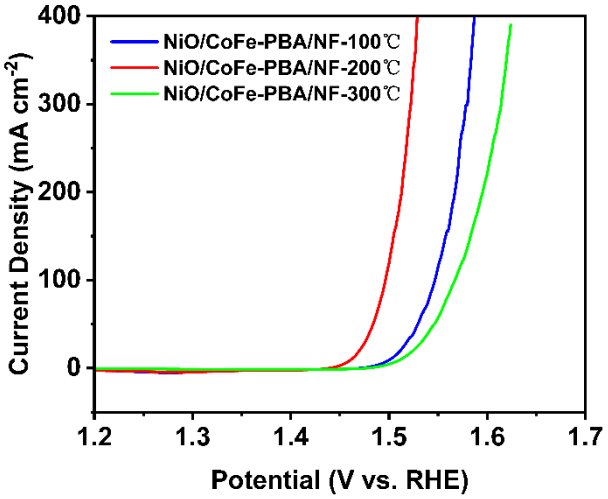

Fig. S9. LSV curves for samples with various temperatures in 1.0 M KOH.

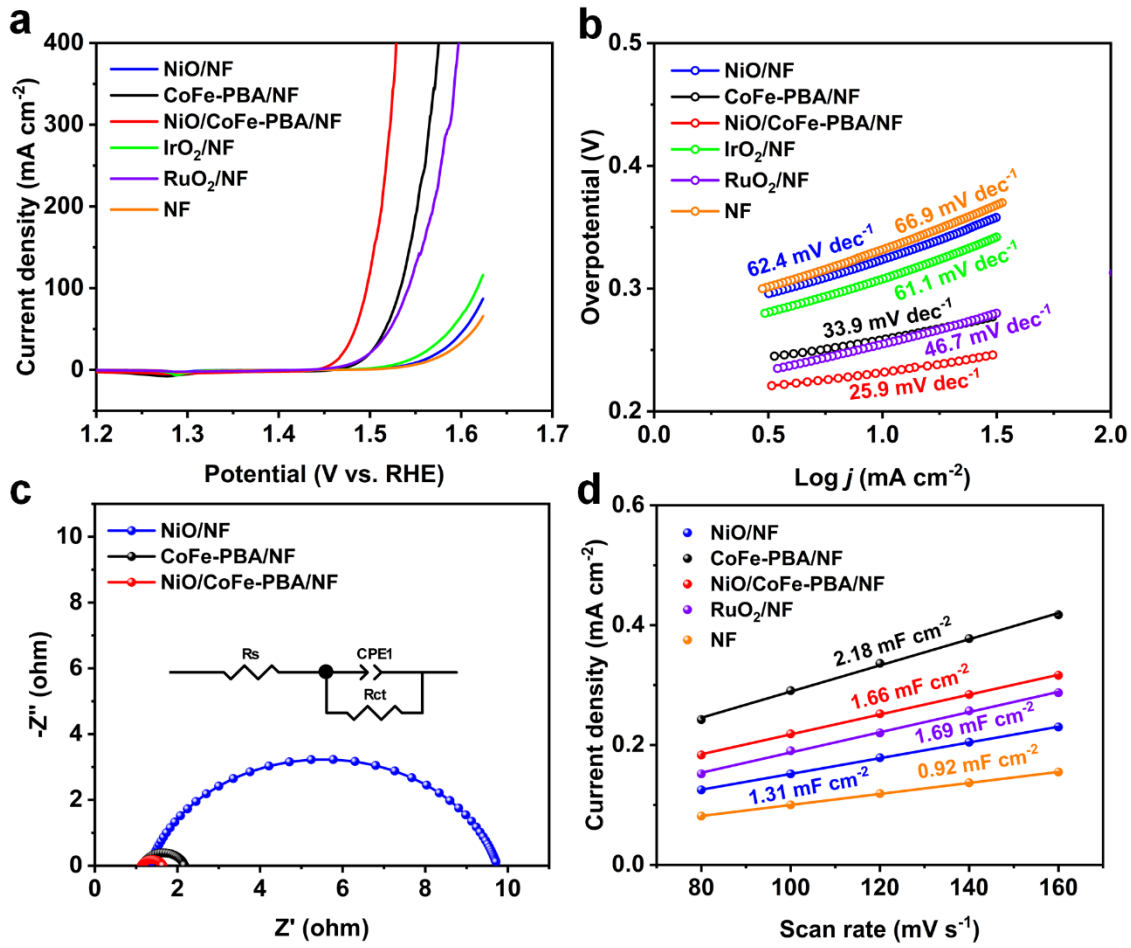

Fig. S10. OER performance in 1.0 M KOH solution. a) LSV curves, and b) the corresponding Tafel plots; c) EIS; d) C_{dl} values.

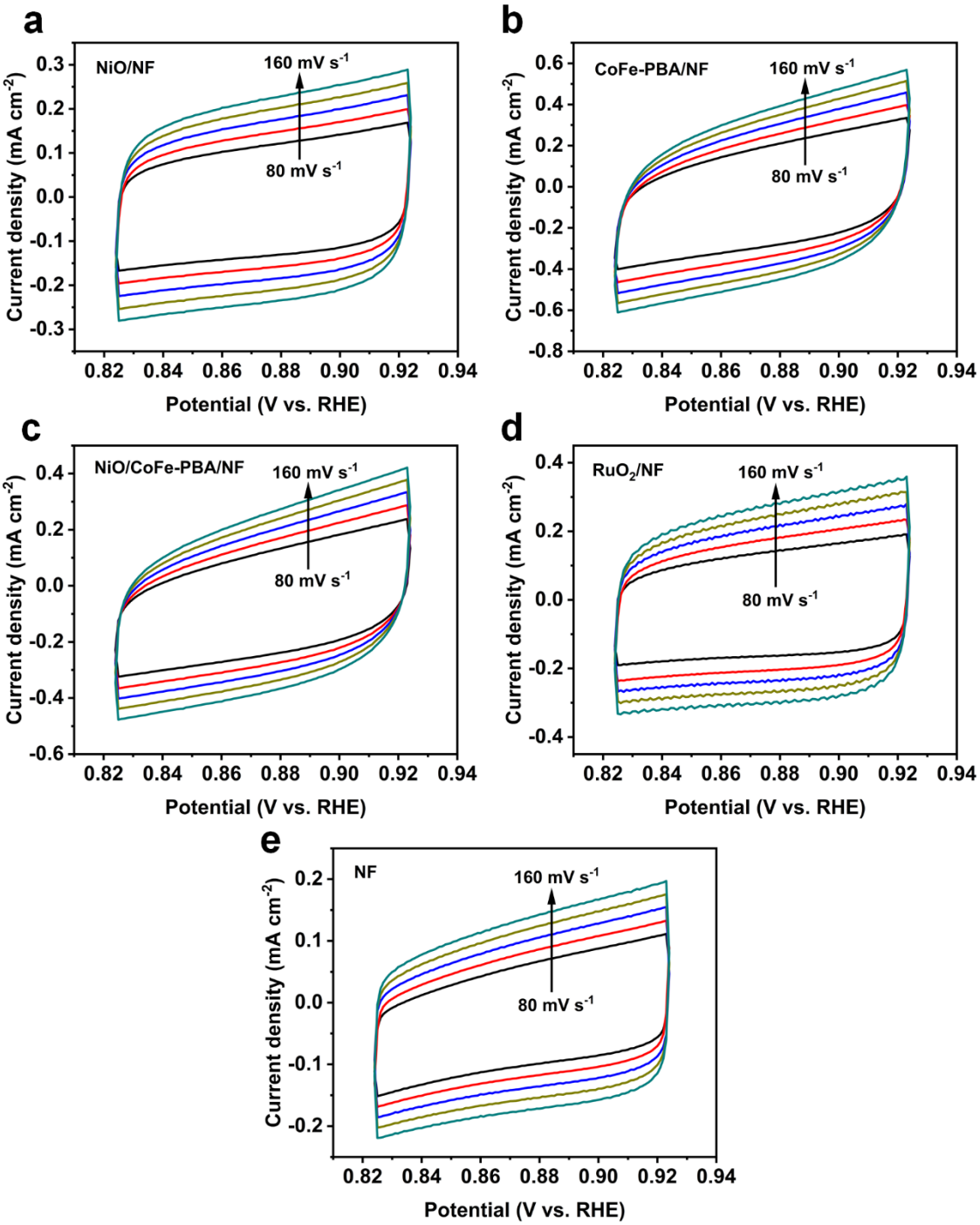

Fig. S11. Cyclic voltammograms at various can rates of 80, 100, 120, 140 and 160 mV s^{-1} for a) NiO/NF, b) CoFe-PBA/NF, c) NiO/CoFe-PBA/NF, d) RuO_2/NF, and e) NF in 1.0 M KOH solution.

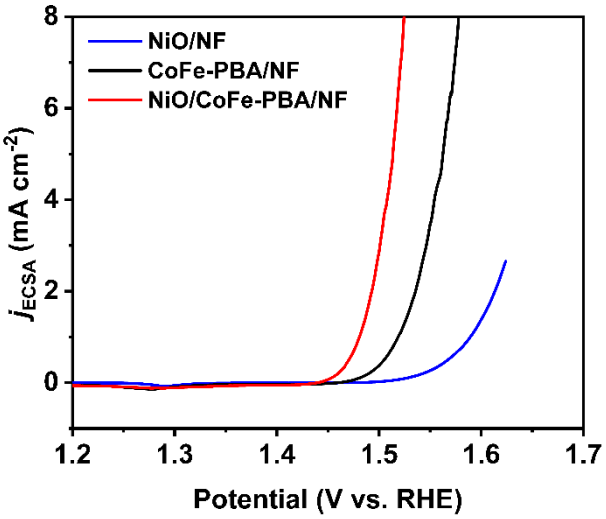

Fig. S12. ECSA-normalized LSV curves in 1.0 M KOH solution.

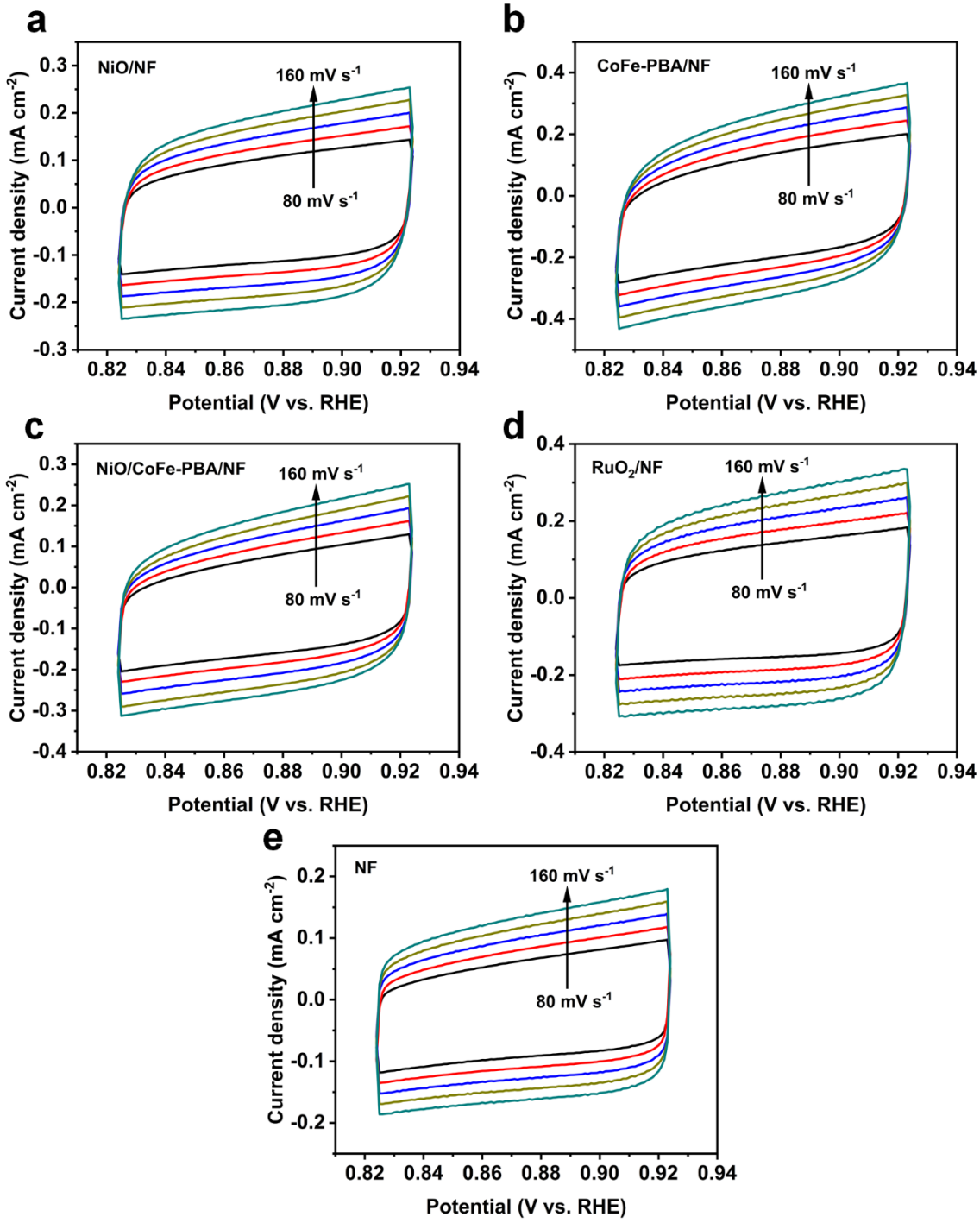

Fig. S13. Cyclic voltammograms at various can rates of 80, 100, 120, 140 and 160 mV s^{-1} for a) NiO/NF, b) CoFe-PBA/NF, c) NiO/CoFe-PBA/NF, d) RuO_2/NF, and e) NF in 1.0 M KOH with seawater solution.

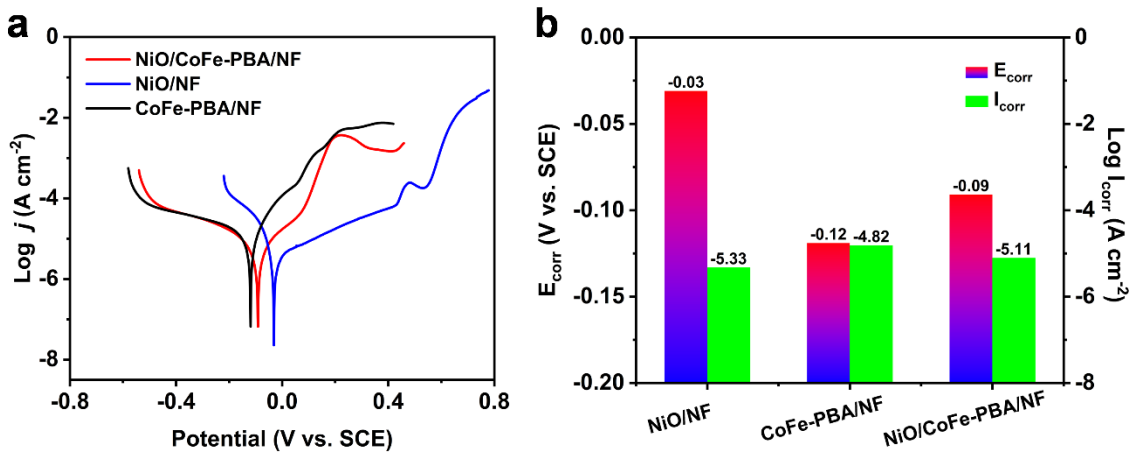

Fig. S14. a) Corrosion polarization curve, and b) the corresponding corrosion potential (E_{corr}) and corrosion current density (I_{corr}).

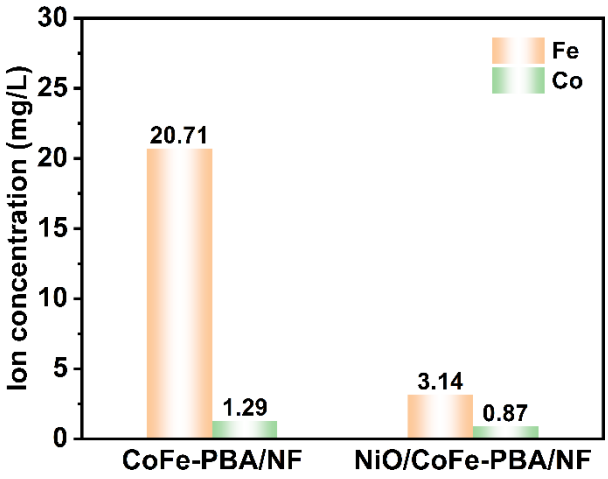

Fig. S15. Ion concentration of Fe and Co in 1.0 M KOH with seawater solution after stability test.

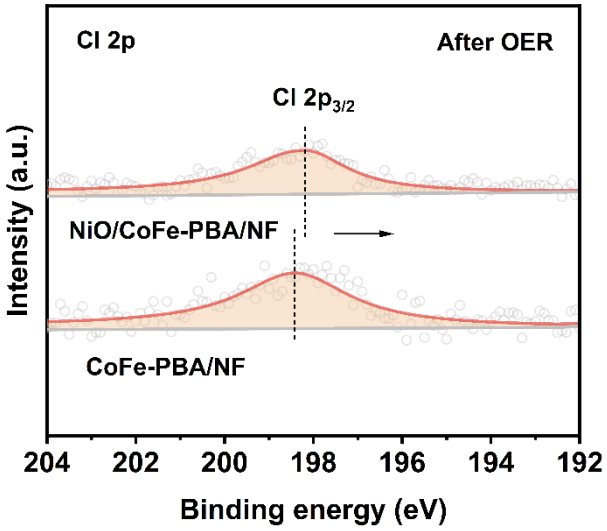

Fig. S16. High-resolution XPS spectra of Cl 2p for CoFe/PBA/NF and NiO/CoFe-PBA/NF after OER test.

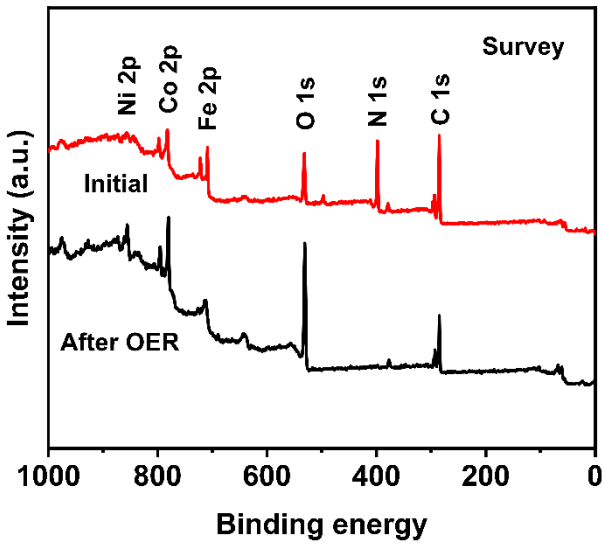

Fig. S17. XPS survey spectra of NiO/CoFe-PBA/NF after OER test.

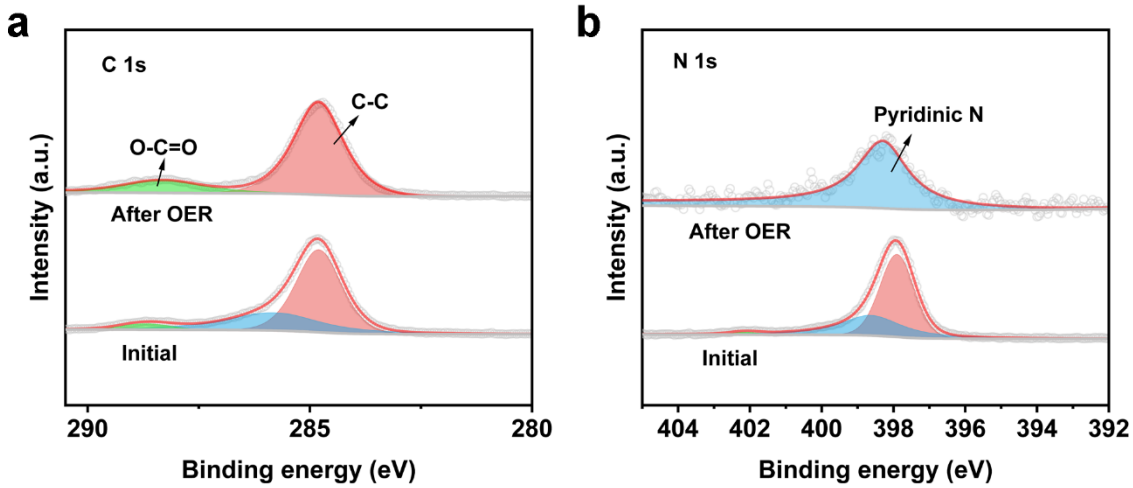

Fig. S18. High-resolution XPS spectra of NiO/CoFe-PBA/NF after OER test. a) C 1s, and b) N 1s.

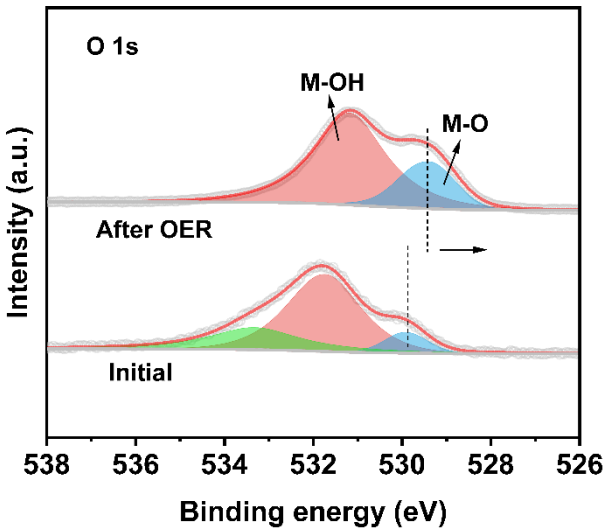

Fig. S19. High-resolution XPS spectra of O 1s for NiO/CoFe-PBA/NF after OER test.

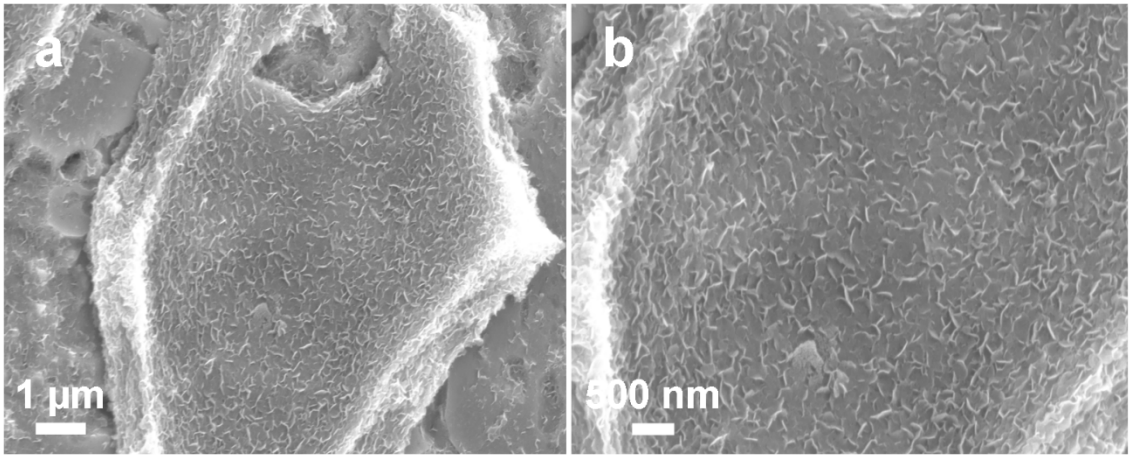

Fig. S20. SEM images of NiO/CoFe-PBA/NF after OER test.

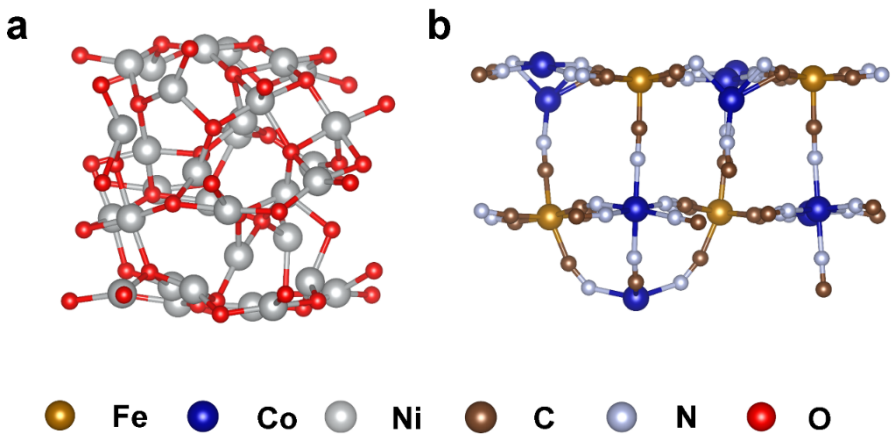

Fig. S21. The structural feature of a) NiO and b) CoFe-PBA.

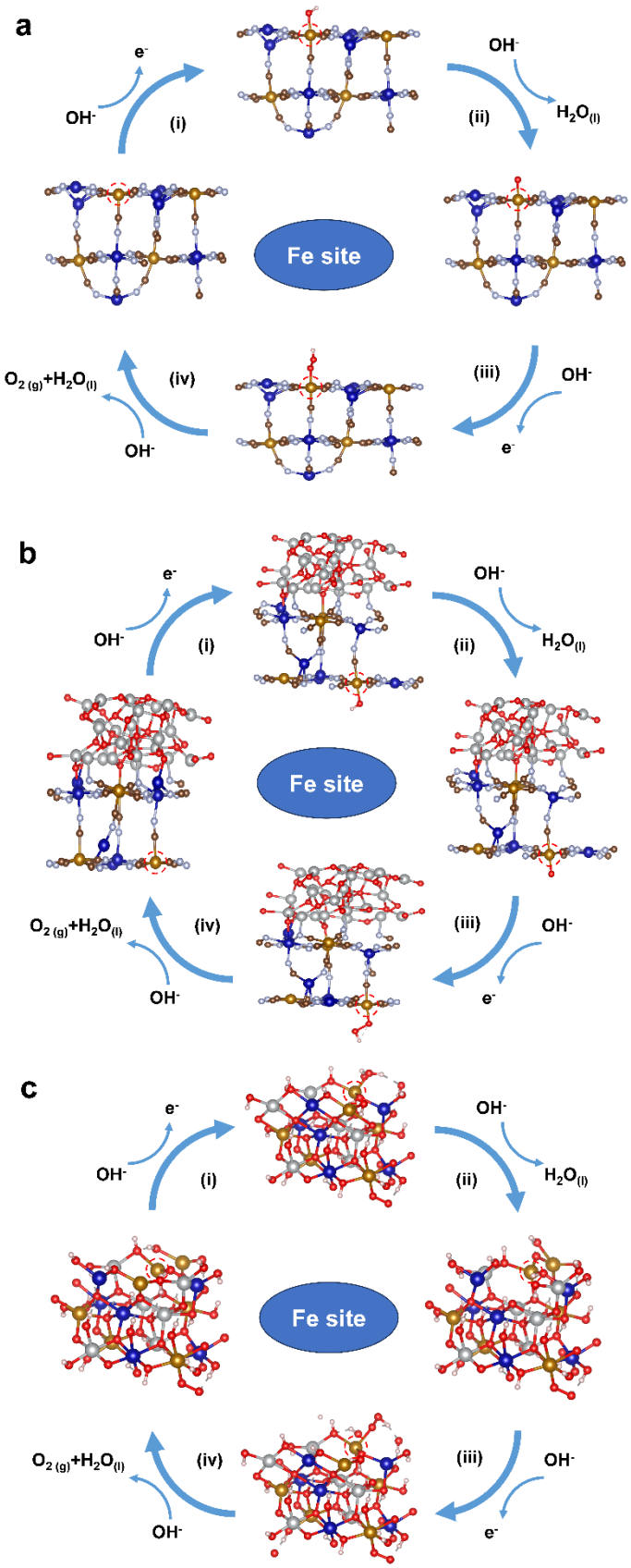

Fig. S22. Four-electron mechanism of OER on the Fe sites in a) CoFe-PBA, b) NiO/CoFe-PBA and c) FeCoNiOOH.

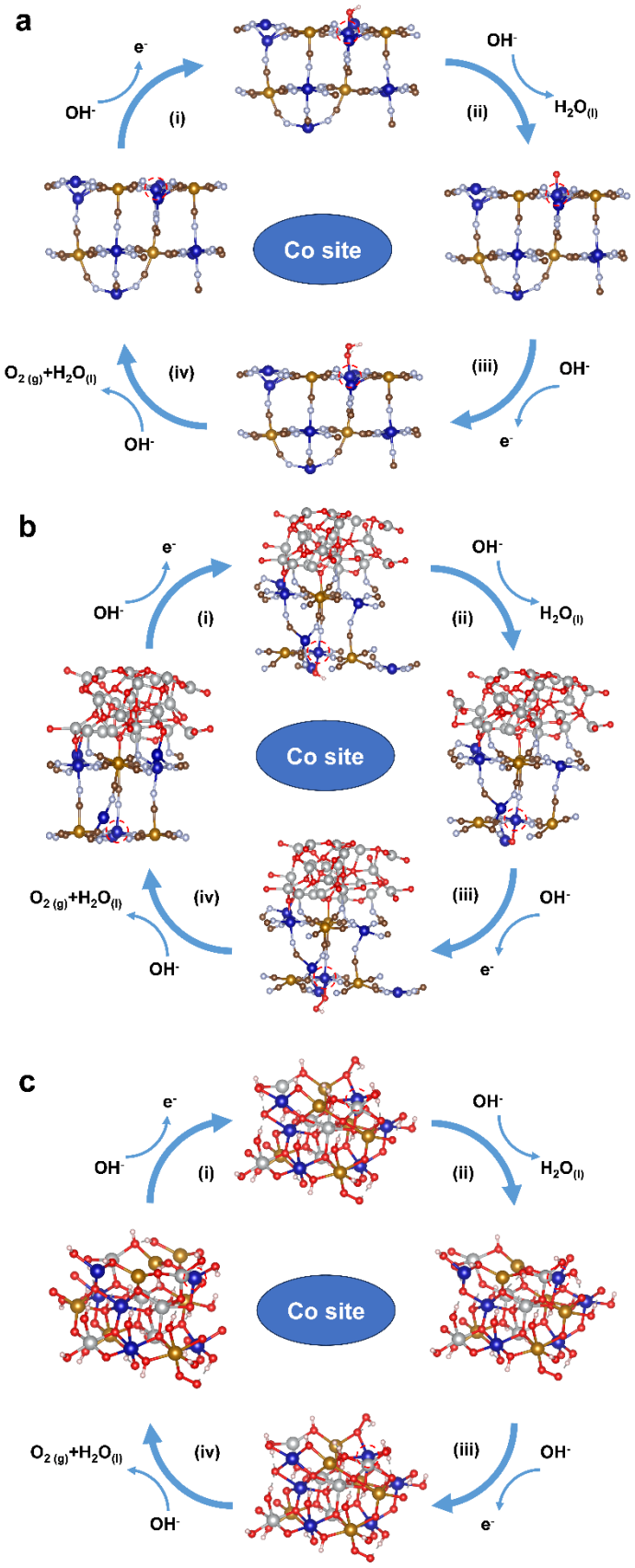

Fig. S23. Four-electron mechanism of OER on the Co sites in a) CoFe-PBA, b) NiO/CoFe-PBA and c) FeCoNiOOH.

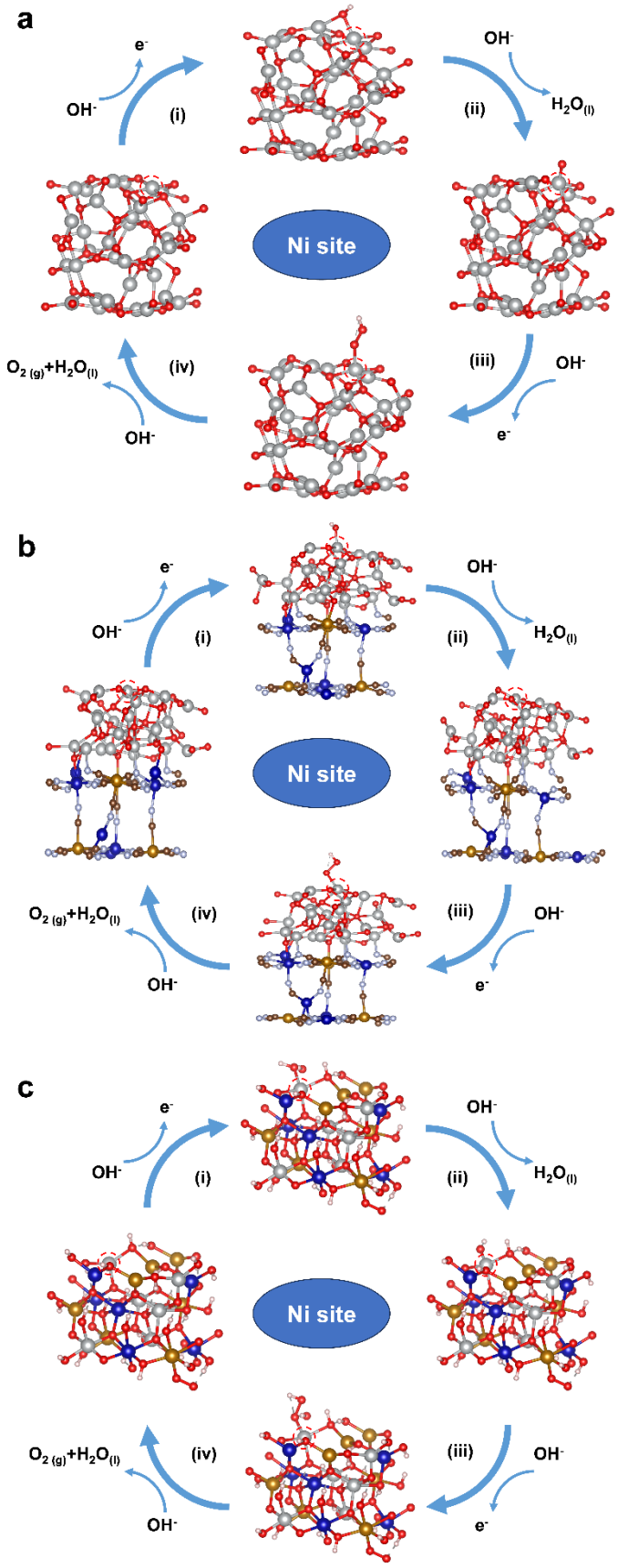

Fig. S24. Four-electron mechanism of OER on the Ni sites in a) NiO, b) NiO/CoFe-PBA and c) FeCoNiOOH.

Table S1. EIS calculation parameters of NiO/NF, CoFe-PBA/NF, and NiO/CoFe-PBA/NF for OER in 1 M KOH solution.

Sample	NiO/NF	CoFe-PBA/NF	NiO/CoFe-PBA/NF
R_s (Ω)	1.329	1.162	1.129
R_{ct} (Ω)	8.413	1.007	0.5194
CPE-T (Ω)	0.0173	0.2196	0.2351
CPE-P (Ω)	0.8348	0.8336	0.7799

Table S2. EIS calculation parameters of NiO/NF, CoFe-PBA/NF, and NiO/CoFe-PBA/NF for OER in 1 M KOH with seawater solution.

Sample	NiO/NF	CoFe-PBA/NF	NiO/CoFe-PBA/NF
R_s (Ω)	1.876	1.169	1.212
R_{ct} (Ω)	26.42	3.756	1.019
CPE-T (Ω)	0.0171	0.2847	0.2099
CPE-P (Ω)	0.8059	0.7751	0.7862

Table S3. Comparison of the OER performance in 1.0 M KOH with seawater for different electrocatalysts.

Catalysts	Overpotential @100 mA cm^{-2}	electrolyte	iR Compensation (%)	Ref.
NiO/CoFe-PBA/NF	**301 mV**	**1.0 M KOH + Seawater**	**85**	**This work**
NiFe-LDH/MOF	307 mV	1.0 M KOH + Seawater	100	4
FeOOH-(CrCo)O_x/PCF	306 mV	1.0 M KOH + Seawater	90	5
Mo-Ni_3S_2/VO_2	316 mV	1.0 M KOH + Seawater	85	6
NiMoS@NSC/NF	318 mV	1.0 M KOH + Seawater	90	7
Ni/$Co(OH)_2$-Ru@NF	324 mV	1.0 M KOH + Seawater	80	8
NiFe-MOF@Ni_2P/$Ni(OH)_2$	302 mV	1.0 M KOH + Seawater	85	9
Ni_3S_2@NiFe-TDC-60	380 mV	1.0 M KOH + Seawater	without	10
S-$NiMoO_4$@NiFe-LDH	315 mV	1.0 M KOH + Seawater	90	11
NiCoHPi@Ni_3N/NF	365 mV	1.0 M KOH + Seawater	85	12
NiFeP/Ni_3S_2	406 mV	1.0 M KOH + Seawater	85	13

Table S4. The Gibbs free energy diagram of the possible four steps of the OER process on the Fe site of CoFe-PBA, NiO/CoFe-PBA and FeCoNiOOH.

Sample	CoFe-PBA	NiO/CoFe-PBA	FeCoNiOOH
*→*OH	0.71 eV	0.39 eV	0.44 eV
*OH→*O	1.25 eV	1.49 eV	1.22 eV
*O→*OOH	1.98 eV	1.70 eV	1.68 eV
OOH→+O_2	0.98 eV	1.34 eV	1.57 eV

Table S5. The Gibbs free energy diagram of the possible four steps of the OER process on the Co site of CoFe-PBA, NiO/CoFe-PBA and FeCoNiOOH.

Sample	CoFe-PBA	NiO/CoFe-PBA	FeCoNiOOH
***→*OH**	0.47 eV	0.53 eV	0.91 eV
***OH→*O**	2.25 eV	1.49 eV	1.23 eV
***O→*OOH**	0.92 eV	2.03 eV	1.88 eV
***OOH→*+O_2**	1.27 eV	0.87 eV	0.89 eV

Table S6. The Gibbs free energy diagram of the possible four steps of the OER process on the Ni site of CoFe-PBA, NiO/CoFe-PBA and FeCoNiOOH.

Sample	NiO	NiO/CoFe-PBA	FeCoNiOOH
***→*OH**	1.41 eV	1.06 eV	0.50 eV
***OH→*O**	1.92 eV	0.29 eV	1.62 eV
***O→*OOH**	1.45 eV	1.81 eV	1.50 eV
***OOH→*+O_2**	0.14 eV	1.76 eV	1.31 eV

References

1. G. Kresse and D. Joubert, From ultrasoft pseudopotentials to the projector augmented-wave method, *Phys. Rev. B*, 1999, **59**, 1758-1775.
2. J. P. Perdew, K. Burke and M. Ernzerhof, Generalized Gradient Approximation Made Simple, *Phys. Rev. Lett.*, 1996, **77**, 3865-3868.
3. C. Yue, L. Wang, H. Wang, J. Du, M. Lei and M. Pu, First-Principles Study on the Electrocatalytic Oxygen Evolution Reaction on the (110) Surfaces of Layered Double Hydroxides, *J. Phys. Chem. C*, 2022, **126**, 18351-18365.
4. M. Xiao, C. Wu, J. Zhu, C. Zhang, Y. Li, J. Lyu, W. Zeng, H. Li, L. Chen and S. Mu, In situ generated layered NiFe-LDH/MOF heterostructure nanosheet arrays with abundant defects for efficient alkaline and seawater oxidation, *Nano Res.*, 2023, **16**, 8945-8952.
5. R. Liu, G. Chen, Y. Guo, T. Li, J. Qiu, B. He and P. Tang, Designing persimmon-liked FeOOH-(CrCo)O_x on the plasma-treated cobalt foam for a highly efficient oxygen evolution in an alkaline-seawater electrolyte, *Chem. Eng. J.*, 2024, **500**, 157098.
6. H. T. Dao, S. Sidra, V. H. Hoa, Q. H. Nguyen, M. Mai, P. K. L. Tran and D. H. Kim, In situ growth and interfacial reconstruction of Mo-doped Ni_3S_2/VO_2 as anti-corrosion electrocatalyst for long-term durable seawater splitting, *Appl. Catal., B*, 2025, **365**, 124925.
7. Y. He, Y. Hu, Z. Zhu, J. Li, Y. Huang, S. Zhang, M. S. Balogun and Y. Tong, High-performance multidimensional-structured N-doped nickel modulated Mo_2N/FeO_xN_y bifunctional electrocatalysts for efficient alkaline seawater splitting, *Chem. Eng. J.*, 2024, **489**, 151348.
8. Q. Wang, Y. Du, Y. Gong, W. Xiao, H. Li, Y. Du, G. Xu, Z. Wu and L. Wang, Phosphorous and cations boost the electrocatalytic performances of Cu-based compounds for hydrogen/oxygen evolution reactions and overall water-splitting, *Chem. Eng. J.*, 2024, **489**, 151322.
9. J. Liu, J. Yang, Y. Song, J. Sun, Y. Tian, Q. Chen, X. Zhang and L. Zhang, Introducing non-bridging ligand in metal-organic framework-based electrocatalyst enabling reinforced oxygen evolution in seawater, *J. Colloid Interface Sci.*, 2023, **643**, 17-25.
10. G. Zuo, Z. Li, C. Wang, L. Guo and Y. Wang, Mildly sulfurized metal-organic frameworks-derived nickel sulfide heterostructures as bifunctional catalysts for efficient water/seawater electrolysis, *J. Colloid Interface Sci.*, 2025, **700**, 138647.
11. H. Wang, L. Chen, L. Tan, X. Liu, Y. Wen, W. Hou and T. Zhan, Electrodeposition of NiFe-layered double hydroxide layer on sulfur-modified nickel molybdate nanorods for highly efficient seawater splitting, *J. Colloid Interface Sci.*, 2022, **613**, 349-358.
12. H. Sun, J. Sun, Y. Song, Y. Zhang, Y. Qiu, M. Sun, X. Tian, C. Li, Z. Lv and L. Zhang, Nickel–Cobalt Hydrogen Phosphate on Nickel Nitride Supported on Nickel Foam for Alkaline Seawater Electrolysis, *ACS Appl. Mater. Interfaces*, 2022, **14**, 22061-22070.
13. Y. Song, X. Zhang, Z. Xiao, Y. Wang, P. Yi, M. Huang and L. Zhang, Coupled amorphous NiFeP/cystalline Ni_3S_2 nanosheets enables accelerated reaction kinetics for high current density seawater electrolysis, *Appl. Catal., B*, 2024, **352**, 124028.